HQ GRANT
IN-90-CR
234868
P-30

NUMERICAL STUDY OF THE CURRENT SHEET AND PSBL IN A MAGNETOTAIL MODEL

I. DOXAS

Department of Astrophysical, Planetary and Atmospheric Sciences

University of Colorado

Boulder, CO 80309

W. HORTON, K. SANDUSKY, T. TAJIMA and R. STEINOLFSON

Institute for Fusion Studies

University of Texas at Austin

Austin, TX 78712

NAGW-1176

Abstract

A test particle code is used to study the response of ensembles of particles to a two-dimentional, time-dependent model of the geomagnetic tail, and test the proposition (Coroniti, 1985a,b; Büchner and Zelenyĭ, 1986; Chen and Palmadesso, 1986; Martin, 1986) that the stochasticity of the particle orbits in these fields is an important part of the physical mechanism for magnetospheric substorms. The realistic results obtained for the fluid moments of the particle distribution with this simple model, and their insensitivity to initial conditions, is consistent with this hypothesis.

(NASA-CR-183289) NUMERICAL STUDY OF THE CURRENT SHEET AND PSBL IN A MAGNETOTAIL MODEL (Colorado Univ.) 30 p CSCL 03B

N90-11669

G3/90 Unclas 0234868

I Introduction

Since Dungey (1961) posed the problem of magnetic field line reconnection in the Earth's magnetotail a search has been on for a mechanism that would allow the release of the stored magnetic energy, leading to a magnetospheric substorm. The tearing mode is a popular candidate, but since the magnetotail is highly collisionless, we cannot count on collisions to provide the dissipation necessary for the instability, and the reconnection time given by resistive MHD theory (Furth et. al. 1963) is several orders of magnitude too long. Therefore, either a collisionless resistivity is required or a mechanism of an ideal MHD type for reconnection, such as the coalescence instability. We focus on the former in the present paper. In the search for that resistivity two broad approaches can be identified: a search for a dynamical collisionless resistivity and a search for a turbulent collisionless resistivity. In the former, the finite coherence time (the time during which the current carriers are coherently accelerated by the electric field, also called the decorrelation time) arises from single particle dynamics in the magnetotail fields, while in the latter it comes from the scattering of the particles by the modes of the current carrying plasma. In the present work we consentrate on dynamical collisionless resistivity. Several mechanisms have been proposed for turbulent collisionless resistivity (eg. Hagege et. al., 1973; Huba et. al., 1978; Drake and Lee, 1977; Esarey and Molvig, 1987), but recent results form the ISEE-1 and ISEE-2 satellites on the CDAW-6 substorm (Anderson, 1984; Dusenbery, 1989) indicate that wave intensities in the current sheet are insufficient to account for the observed reconnection rate and, in addition, most wave intensities decrease dramatically at the center of the current sheet, making it even harder for turbulence to produce the required resistivity.

Measurements of the particle distribution function by the ISEE-1, ISEE-2 and ISEE-3 satellites indicate the presence of unmagnetized ion orbits in the plasma sheet and the earthward flowing ion streams in the plasma sheet boundary layer (PSBL). On the basis

of these data, Lyons and Nishida (1988) recently suggested that the onset of the neutral line earthward of $80R_e$ involves the details of this diffusion zone in the plasma sheet where the ion motion is non-adiabatic. Their suggestion is that the neutral line must form in this ion diffusion-like zone and that this plasma is also the source of the observed earthward streaming ions. In addition, Chen and Palmadesso (1986), Martin (1986) and Büchner and Zelenyi (1986), recently demonstrated using a variety of techniques (Poincaré surface of section plots, Lyapunov exponents, separatrix crossing) the stochastic nature of the particle orbits in the parabolic field lines of the geomagnetic tail. As is shown in Part-II below, the stochasticity arises from the resonance overlap of the nonlinear current sheet cyclotron oscillations in the reversed tail-earthward field with the cyclotron motion in the weak northward dipole field component B_z. Coroniti (1985a) and Büchner and Zelenyĭ (1987) also proposed substorm models that rely entirely on single particle dynamics.

In view of these new developments, we have undertaken a study of the dynamics and transport of particles in the parabolic field lines of the geomagnetic tail in the presence of a neutral line, at a distance of 25-35 R_e, produced by a reconnection mode perturbation. We advance ensembles of particles with a test particle code, so that no collective effects are present other, than the ones implicit in the assumption that the overall MHD picture is correct (eg. Steinolfson and Van Hoven, 1984) and the perturbation is given by a reconnection mode. All the phenomena we observe are the result solely of the dynamics of ensembles of charged particles in the model fields. The electric and magnetic fields in the geomagnetic tail are modeled by

$$\begin{aligned} B_x &= B_0 \tanh\left(\frac{z}{a}\right) \\ B_z &= B_0 b_0 + B_0 \psi_0 k \sin(kx) e^{\gamma t} \\ E_y &= B_0 \psi_0 \frac{\gamma}{c} \cos(kx) e^{\gamma t} \end{aligned} \tag{1}$$

with x, y, z the usual magnetotail coordinates. These fields can be derived from the magnetic flux function

$$\psi = B_0[a \ln(\cosh(z/a)) + \psi_0 \cos(kx)e^{\gamma t} - b_0 x] \tag{2}$$

where the vector potential is $\vec{A} = -\psi(x, z, t)\hat{e}_y$ and the fields are given by $\vec{B} = \hat{y} \times \nabla\psi$ and $E_y = (1/c)\partial_t\psi$. In the above expressions B_0 is the magnitude of the asymptotic (far from the neutral sheet) horizontal field, a the scale length of the horizontal field, b_0 the normal (northward) magnetic field component, ψ_0 is the amplitude of the tearing perturbation, γ its growth rate and k its wavenumber. The electromagnetic perturbation in Eq. (2) is the standard tearing mode perturbation well studied in resistive MHD simulations (eg. Steinolfson and Van Hoven, 1984). The neutral line occurs when $B_z = -d\psi/dx = 0$, i.e. at time t_c

$$t_c = \frac{1}{\gamma} \ln\left(\frac{b_0}{k\psi_0}\right) \tag{3}$$

for the model fields in Eq. (1). For $t \ll t_c$ the field lines are long, open loops.

The particles are advanced in time using the fields given in Eq. (1), and particle density, bulk velocities, temperature and current are measured as a function of x and z. We find that the initial distribution changes little until the neutral line is formed, and then the number density in the vicinity of the X-point drops, a narrow channel of cross-tail current, in phase with the electric field, is formed around the X-point, and the temperature increases in the same narrow channel where the cross-tail current flows, with final temperatures in the range of 1-12 keV. Finally the hot particles are expelled from the vicinity of the X-point into the PSBL, and earthward streaming ions with bulk velocities in the range of 400-1000 km/s are observed there. These results are in good qualitative and quantitative agreement with observed events in the magnetotail. Number density is observed to decrease with a simultaneous increase in temperature after substorm onset,

with temperatures in the range of 1-10 keV (eg. Paschmann et. al., 1985; Huang, 1989), and earthward streaming ions with velocities of several hundred km/s are observed in the PSBL (eg. DeCoster and Frank, 1979; Eastman et. al., 1984). The agreement of our results, which were obtained with a test particle code, with the observations lends support to the proposition (Coroniti, 1985a; Büchner and Zelenyĭ, 1986; Martin, 1986) that single particle dynamics play an important role in determining the behavior of the geomagnetic tail.

II Previous Work

Harris (1962) solved the Vlasov equation for the case of a reversing one-dimensional magnetic field, a configuration often used as a zeroth order approximation to the magnetotail fields. More realistic approximations include a cross-tail electric field and/or a small normal magnetic field component, and many authors have studied the dynamics of single particles in these model fields (eg. Parker, 1957; Speiser, 1965, 1967, 1968, 1970; Schindler, 1965; Sonnerup, 1971; Eastwood, 1972, 1974; Lyons and Speiser, 1982; Kim and Cary, 1983; Speiser and Lyons, 1984; Martin, 1986; Büchner and Zelenyĭ, 1986, 1987). The first attempt to calculate a collisionless resistivity, and hence the tearing mode growth rate, was made by Coppi et. al. (1966) and Laval et. al. (1965) for a one-dimensional Harris sheet. They found the system unstable to the electron tearing mode, but the growth time was unrealistically long for magnetospheric parameters, $\sim$ 4.5 days. The more realistic case of a two-dimensional magnetic field (a small B_z added) was first studied by Galeev and Zelenyĭ (1976) (see also Galeev, 1979) who found that, as was proposed by Schindler (1974), the electron tearing mode is stable in this field geometry. This is due to the fact that the normal magnetic field component magnetizes the electrons in the quasineutral layer (where the horizontal field vanishes) and forces an adiabatic response to the tearing perturbation. The electron Landau interaction, which provides the dissipation necessary for the growth

of the tearing mode in the one-dimensional case, is inhibited and the mode is therefore stable. From the energy balance point of view, the energy required to produce the adiabatic electron response to the tearing mode exceeds the free energy available in the current sheet (Coroniti, 1980; Lembège and Pellat, 1982). Furthermore, the calculation of Lembège and Pellat (1982), which included the effects of the particle drift in the normal field as well as a finite Larmor radius, showed that the adiabaticity of the electrons will even stabilize the *ion* tearing mode, which was proposed by Schindler (1974) as an alternative to the electron tearing mode, and the growth rate of which was calculated by Galeev and Zelenyĭ (1976). It was therefore becoming important to search for a mechanism that could destabilize the electron tearing mode.

As was mentioned earlier this search can be divided into two broad categories; dynamical or inertial resistivity and turbulent or collective resistivity. Coroniti (1980) first considered the effects of turbulence-induced pitch-angle scattering of the electrons on the growth rate of the electron tearing mode, and found that pitch-angle diffusion makes the mode unstable. Many authors (eg. Hagege et. al., 1973; Huba et. al., 1978; Drake and Lee, 1977; Esarey and Molvig, 1987) have considered the effects of different types of turbulence (lower hybrid drift wave turbulence, ion acoustic turbulence, broadband electrostatic noise) and they all cause the electron tearing mode to become unstable. Turbulence is indeed present in the geomagnetic tail, but it is either in the wrong place (broadband electrostatic noise, for example, is mostly confined to the PSBL) or of insufficient magnitude. In addition, recent studies (Anderson, 1984; Dusenbery, 1989) show that wave intesity decreases even more at the center of the current sheet. This situation, together with the fact that *all* kinds of random driving considered (including *spatial* rather than velocity-space diffusion) destabilized the electron tearing mode, led to the suggestion (Büchner and Zelenyĭ, 1986; Martin, 1986; Doxas, 1988) that the intrinsic stochasticity of the particle orbits in the magnetotail fields may be sufficient to destabilize the mode.

Kim and Cary (1983) first showed that particle trajectories in the simpler but related geometry of elliptic magnetic flux surfaces can be stochastic. That was also demonstrated for more realistic magnetotail field models by the work of Chen and Palmadesso (1986) who found stochastic regions in phase space. Martin (1986) measured Lyapunov exponents and used them as the effective coherence time τ to calculate the collisionless resistivity. Büchner and Zelenyĭ (1986, 1987) identified

$$\kappa = \frac{B_{z0}}{B_0}\sqrt{\frac{a}{\rho_0}} = \frac{b_0}{\sqrt{\epsilon}} \tag{4}$$

as the parameter that controls the stochasticity of the orbits. In the above expression B_{z0} is the magnitude of the constant normal magnetic field component, B_0 the asymptotic (far from the neutral sheet) value of the horizontal magnetic field, a the scale length of the reversing horizontal field (which is equal to the width of the Harris current sheet) and ρ_0 the particle gyroradius in the asymptotic field B_0. The parameter $\epsilon = \rho_0/a$ is the small parameter in the adiabatic approximation. In the current sheet the parameter κ arises from the ratio of the cyclotron frequency $\omega_{cz} = eB_{z0}/mc$ around the north-south field, to the frequency of the strongly nonlinear vertical oscillations in the reversed earth-tail magnetic field $\omega_{cx}(z) = eB_x(z)/mc$ (eg. Lyons, 1984). The value of κ gives the number of gyrations around the normal field that a particle will execute in one period of the vertical oscillations. For $\kappa \gg 1$ the magnetic moment μ is a good adiabatic invariant, and the adiabatic approximation is valid. For $\kappa \ll 1$ a new adiabatic invariant can be found (Schindler, 1965; Speiser, 1970; Sonnerup, 1971). For $\kappa \approx 1$ however, no adiabatic invariant exists, and the motion is highly stochastic.

III Numerical Results

The equations of motion used to advance the particles are given by the Lorentz force with the fields in Eq. (1). We introduce dimensionless variables by scaling length to the

perturbation wavelength $\lambda = 2\pi/k$, time to the ion gyroperiod in the asymptotic field $T_{0i} = 2\pi/\omega_{0i} = 2\pi(m_i c/eB_0) = 3.277\ sec$, mass to the ion mass and charge to the unit charge e (electrons have charge $-e$). The unit velocity is therefore $v_0 = \omega_{0i}/k = 9.71 \times 10^9\ cm/s$, and the unit current $j_0 = e\rho_n v_0 = 1.55\ \mu A/m^2$, where $\rho_n = 0.1\ cm^{-3}$ is the number density in the magnetotail, and a typical value for the asymptotic field is $B_0 = 20\,nT$ (eg. Lyons and Williams, 1984). From now on all values given for the parameters and all variables in equations will be dimensionless unless otherwise stated. Whenever needed to avoid confusion, the dimensionless quantities will be denoted by a hat (eg. $\hat{x} = x/\lambda$). The system is described by four parameters. The amplitude of the magnetic flux associated with the tearing mode ψ_0, the constant normal magnetic field component b_0, the aspect ratio of the tearing mode $ka(= 2\pi a)$ and its growth rate γ.

We fully resolve the smallest time and space scales in the problem. For the parameters used, the smallest length scale is the particle gyroradius in the asymptotic field, $\rho_0 = v/\omega_0$ with v the total particle velocity. The length scale over which the magnetic field reverses direction, a, is always at least two orders of magnitude larger than ρ even in very high energy test runs, and the wavelength of the tearing perturbation is the longest scale in the system. Approximate values for these parameters in the magnetotail are (eg. Lyons and Williams, 1984) $\lambda = 8\text{-}80\,R_e$ and $a \approx 1\,R_e$ where $R_e = 6380\,km$ is the radius of the Earth. In contrast the electron gyroradius is of the order of a few kilometers, and the ion gyroradius a few hundred kilometers. The smallest timescale is the particle gyroperiod in the asymptotic field $T_0 = 2\pi/\omega_0 = 1$. The only other timescale in the problem is the tearing mode growth time, and the shortest growth time we used was 20 ion gyroperiods.

Sample populations of 16000-64000 particles are advanced in time using a fourth order Runge-Kutta method (eg. W. Gear, 1971; W.H. Press et. al., 1986). Electrons and ions are treated separately so that a realistic ion to electron mass ratio of 1836 can be used.

The electron gyrofrequency is therefore $\omega_{0e} = -1836 \times (2\pi)$. The time step h is chosen so that the particle gyroperiod is adequately resolved and the final (cumulative) error in the particle position $|\delta\vec{x}|$ is much smaller than the particle gyroradius in the asymptotic field. To get an estimate for the error in the particle position, a small percentage of particles ($\sim 1\%$) are also advanced with a sixth order Runge-Kutta and half the timestep. The particle position $\vec{x}_{h/2}$ calculated with the higher order method and shorter timestep is then compared to the position of the particle $\vec{x}_h$ calculated with the regular method and timestep, and the error $|\delta\vec{x}|$ is given by

$$|\delta\vec{x}| = |\vec{x}_{h/2} - \vec{x}_h| \tag{5}$$

The lowest value of T_0/h used in any run is 110, and the lowest value of $\rho/|\delta\vec{x}|$ is of the order of 10^2. The following values of the parameters were used in the runs: the normal magnetic field in the range $0.003 \leq b_0 \leq 0.1$, the amplitude of the tearing mode in the range $4 \times 10^{-4} \leq \psi_0 \leq 0.01$, the tearing mode growth rate in the range $0.005 \leq \gamma \leq 0.05$ and the tearing mode aspect ratio was $\lambda/a = 50$. In order to test heating ireversibility, as well as adress some concerns explained below, we also made a number of runs with a time dependent perturbation amplitude ($\psi_0 \rightarrow \psi_0 e^{\alpha t^2}$ and $\psi_0 \rightarrow \psi_0 \sin(\omega t)$) with $-0.001 \leq \alpha \leq 0.01$ and $0 \leq \omega t \leq \pi$.

The equations of motion are periodic in the x-direction so the particles are kept in a cell with an x-dimension of one, but are allowed to move freely in z. The particles are loaded at $t = 0$ using two different initial distributions; a flat distribution in both velocity and configuration space,

$$-x' \leq x \leq x' \quad , \quad -z' \leq z \leq z' \quad , \quad -v' \leq v_j \leq v' \tag{6a}$$

or a gaussian distribution in x and v,

$$\rho(z, \vec{v}) \sim \frac{1}{\sigma_x \sigma_v^3 (2\pi)^2} e^{-x^2/2\sigma_x} e^{-v^2/2\sigma_v} \quad , \quad -x' \leq x \leq x' \tag{6b}$$

We always start with a flat distribution in x since the equation of motion are periodic in x. The range of initial conditions used in the different computer experiments are $x' = \lambda/2$, z' and σ_z in the range $0.1a \leq z', \sigma_z \leq 2a$, and the velocity space limit v' and deviation σ_v are chosen so that the average kinetic energy of the particles is in the range $2\times10^{-5}\ keV \leq T \leq 2\ keV$. The system is typically advanced for $200-1000$ gyroperiods, which is equivalent to 10–50 minutes for ions and 0.5–2 seconds for electrons. Time enters explicitly the equations of motion exclusively through the combination $\psi_0 e^{\gamma t}$, (we always consider a constant ψ_0, the time dependence is introduced explicitly later) so that a sweep in the value of ψ_0 is equivalent to running longer times, with only the initial conditions distinguishing the two cases. This observation is supported by the simulations and was used in several occasions to shorten lengthy runs. Electron runs were spaced at various times in the 10–50 minute time history of the ions using different values of ψ_0, so that 'snapshots' of the electron behaviour during the ion run were obtained.

We compute and study the average density, velocity (x, y and z-component), current (x, y and z-component), temperature and $\langle \hat{j} \cdot \hat{E} \rangle$ as a function of x and z, at any given time t.

The average velocity is defined by

$$\langle v_j \rangle(s,t) = \frac{v_0}{n} \sum_{i=1}^{n} \hat{v}_j^i = v_0 \langle \hat{v}_j \rangle(s,t) \tag{7}$$

where n is the number of particles whose s-coordinate is in the range $s \rightarrow s+\delta s$ irrespective of the value of the other coordinate, and $\hat{v}_j^i$ is the j-component of the dimensionless velocity of the i^{th} particle in units of the scale velocity $v_0 = \omega_{0i}/k$. Here s represents either x or z.

Using the average velocity, we can define the current by

$$j_j(s,t) = e\rho_p(s)\langle v_j \rangle(s,t) \tag{8}$$

where $\langle v_j \rangle$ is the average velocity of all particles whose s-coordinate has a value between s and $s + \delta s$, and $\rho_p(s)$ is the particle number density in the cell $s \rightarrow s + \delta s$. The number density is in turn given by

$$\rho_p(s) = \rho_n \frac{n}{N \delta s} \tag{9}$$

where n has the same meaning as in Eq. (7), N is the total number of particles in the simulation, $\rho_n = 0.1\, cm^{-3}$ the average number density in the magnetotail and δs the dimensionless cell size. The factor $n/N\delta s$ is a density factor that describes how the density at position s differs from the average magnetotail number density ρ_n. If $n = N\delta s$, then $\rho_p = \rho_n$. With that definition of the density we can now rewrite Eq. (8) as

$$\begin{aligned} j_j(s,t) &= e\rho_p \langle v_j \rangle(s,t) = e\frac{\rho_n n}{N\delta s} v_0 \frac{\sum_{i=1}^{n} \hat{v}_j^i}{n} \\ &= e\rho_n v_0 \left(\frac{1}{N\delta s} \sum_{i=1}^{n} \hat{v}_j^i \right) = j_0 \langle \hat{j}_j \rangle(s,t) \end{aligned} \tag{10}$$

where $j_0 = e\rho_n v_0$ is the scale current.

The in-phase part of the reconnection current $\langle j \cdot \hat{E} \rangle$ is computed by

$$\begin{aligned} \langle j \cdot \hat{E} \rangle_{(s,t)} &= (e\rho_n v_0) \left(\frac{1}{N\delta s} \sum_{i=1}^{n} \hat{v}_y^i \cos(2\pi \hat{x}^i) \right) \\ &= (e\rho_n v_0) \langle \hat{j} \cdot \hat{E} \rangle \end{aligned} \tag{11}$$

and the temperature is given in keV using

$$\begin{aligned} &\frac{1}{2} m \langle v^2 \rangle = \frac{1}{2} m v_0^2 \langle \hat{v}^2 \rangle \\ &\langle \hat{v}^2 \rangle = \left\langle \left(\hat{v}_x - \langle \hat{v}_x \rangle \right)^2 \right\rangle + \left\langle \left(\hat{v}_y - \langle \hat{v}_y \rangle \right)^2 \right\rangle + \left\langle \left(\hat{v}_z - \langle \hat{v}_z \rangle \right)^2 \right\rangle \end{aligned} \tag{12}$$

We have fifteen ion runs and four of the much more expensive electron runs. Although nineteen runs are insufficient for a systematic exploration of the parameter space (there

are four parameters that describe the system, ψ_0, b_0, ka and γ), their qualitative results are very similar even for widely different values of the parameters and initial conditions, and we feel that we can draw broad conclusions about the behavior of the system even from a limited sample. We will go here in detail through two runs (one for ions and one for electrons) that exhibit the main behavior patterns of the system.

For the ion run, the dimensionless variables are $\psi_0 = 0.001$, $b_0 = 0.05$, $\gamma = 0.01$, and $a = 0.02$. Substituting these values into Eq. (3), we find that the neutral line will appear at time $t = 207.4$ (the dimensionless time is in units of ion gyroperiods, $T_{0i} = 2\pi/\omega_{0i} = 3.28\ sec$). In Fig. (1) we show plots of the magnetic field lines, with a sample 200 particles superimposed, for three different times during the run. The dashed vertical lines are located at $z = \pm a$. As we see in Fig. (1)-a, the particles are loaded at time $t = 0$ with a flat distribution between $z = -a$ and $z = a$, ($z' = a$ in Eq. (6)) and over a whole wavelength in x ($x' = \lambda/2$). The initial velocity distribution is also flat in all velocity components ($-v'_j < v_j < v'_j$) with $v'_j = 1.4 \times 10^{-4}$, equivalent to an initial temperature of only $0.8\ eV$. As we shall see, even this run, with a very low initial temperature, will give results similar to runs with initial temperature close to the observed temperature.

The initial distribution changes little until shortly before the neutral line forms. In Fig. (1)-b we show a plot of the magnetic field lines with 200 sample particles superimposed at time $t = 183.3$, less than 25 ion gyroperiods before the neutral line appears. We see that the area around $x = -\lambda/4$, where the neutral line is first going to form, is thinning out, while all particles have been expelled from the centers of the magnetic islands at the top and bottom of the picture. In Fig. (1)-c we see the same area at time $t = 233.3$, only 26 gyroperiods after the appearance of the neutral line. We see that the area around the neutral line is almost depleted. Still, most particles are within the $z = \pm a$ boundaries they were placed in at $t = 0$. Fig. (1)-d shows the fields and particles at $t = 280.0$. All

particles have been expelled from the neutral line area, and they are following the magnetic field lines, as the magnetic island expands, into the PSBL. Our run is terminated shortly afterwards, since we can no longer make any meaningful measurements of the current or temperature in the neutral line area. It is interesting to note how remarkably little happens in the 180 or so gyroperiods ($\sim 10\ min$) at the beginning of the run, while most changes take place within 50-70 gyroperiods ($\sim 3\ min$) around the appearance of the neutral line.

The in-phase current $\langle \hat{j} \cdot \hat{E} \rangle$ and the particle temperature is plotted in Figure (2) as a function of z for three different times. The initial distribution is again essentially unchanged for the beginning of the run. As we see in Figs. (2)-a,b, at time $t = 166.7$ there is a well defined current channel in z, and the temperature has increased by a factor of 3–4 in the same narrow channel in which the current flows. Notice that the temperature profile in z has just developed a new narrow channel around $z = 0$, where the temperature is going to increase dramatically between now and the appearance of the neutral line. Figs. (2)-c,d show the current and temperature at time $t = 216.7$, just nine gyroperiods after the appearance of the neutral line. The temperature in the narrow channel around the reversal layer has increased by almost an order of magnitude, while the rest of the temperature profile in z has broadened even more. Finally in Figs. (2)-e,f we show the current and temperature profiles at time $t = 273.3$. Although some current is still flowing, it will soon disappear as the last few remaining particles are being expelled from the area. The temperature profile in z has already crashed in the center, with all the energetic particles expelled from the center and injected into the PSBL where the temperature is now a few keV. Figs. (2)-g,h show the in-phase current $\langle \hat{j} \cdot \hat{E} \rangle$ and the particle temperature at $t = 166.7$ plotted against x. The current profile has developed a sharp gradient at the point where the neutral line is going to appear (at $x = -\lambda/4$) and the temperature profile follows it closely, with high temperatures confined to earthward of the neutral line. Both the magnitude of the in-phase current and the temperature increase after the appearance

of the neutral line, but the profiles remain essencially unchanged until the particles are expelled from the neutral line region.

Although we start with an extremely low temperature ($0.8\,eV$), we end up with temperatures of a few keV, comparable to the actual temperatures in the tail. When we start with more realistic temperatures, (eg. 1.0 keV) the overall heating is much lower than the four orders of magnitude we saw in this run, and the final temperature is a little higher (8–10 keV) but still close to the observed values. If we start the run at a time closer to the time the neutral line appears (by using a larger ψ_0) the system still ends up with approximately the same temperature. This tendency of the system to end up at essentially the same state around the time of the appearance of the neutral line is general and not confined to the temperature, as we already noticed with the density.

In Fig. (3) we show the time history of the x (earthward-tailward) component of the particle velocity. At $t = 33.3$, there is a small (approximately 15 km/sec) earthward drift in a narrow channel around the reversal layer at $z = 0$ (Fig. (3)-a). At later times, both before (Fig. (3)-b) and shortly after the appearance of the neutral line (Fig. (3)-c), the channel gets a little wider and the velocity is higher, but still quite low, of the order of 40–80 km/sec. The narrow depression around $z = 0$ is present in almost all our simulations, and is probably due to the fact that the particles follow so-called Speiser orbits. As they gyrate around B_x (Speiser, 1965) their average x-velocity is zero ($\int_0^\pi v_\perp \cos\theta d\theta = 0$). The depression does not go to zero in our plots because we sample over a finite width in z. After the particles are expelled from the neutral line region and into the PSBL (Fig. (3)-d) the earthward streaming velocity rises quickly to approximately 900 km/sec. Notice how the earthward velocity of the particles stays almost unchanged for the 200 T_{0i} before the neutral line appears, and then sudenly, in only 80 T_{0i}, it increases by more than an order of magnitude. Again, as in the case of the particle temperature, the qualitative picture is

insensitive to initial conditions, and again most of the change comes after the neutral line has formed.

Finally, for the ion run, we show in Fig. (4) contour plots of the particle distribution function for the five boxed areas of particle concentration in Fig. (1)-c. Figs. (4)-a,-d correspond to the four 'arms' of particle concetration clockwise from the top left ($-1.5 \leq z/a \leq 0.$, $0.2 \leq x/\lambda \leq 0.5$, etc.). Fig. (4)-e corresponds to the particle concetration earthward from the neutral line at $-0.5 \leq z/a \leq 0.5$, $-0.2 \leq x/\lambda \leq 0.2$. The figure demonstrates once again the importance of the neutral line, since stochastic velocity-space diffusion is seen to occur only in its vicinity. Since the particle distribution function is broadenning, the figure also provides evidence that the tremendous rise in temperature we observe is real heating, and not the artifact of some unusual distribution function, or a reversible flow of energy from the fields to the particles. The question of reversibility is an important one, and will be addressed in more detail later.

The above scenarios for the changes in the density, bulk velocity and temperature are in good agreement with observations. Earthward streaming ions with speeds up to 40 km/s have been observed in the plasma sheet shortly after substorm onset (eg. Paschmann et. al., 1985), while earthward streaming ions with speeds of 100-900 km/s have been observed in the PSBL (eg. DeCoster and Frank, 1979; Eastman et. al., 1984). The ion temperature is also seen to increase with a simultaneous decrease in density shortly after onset (eg. Paschmann et. al., 1985; Huang, 1989) and ion temperatures in the plasma sheet are in the range 1-10 keV, although the temperatures observed in the PSBL ($\approx 1\,keV$) are lower than those seen in the simulations.

For the electron run the dimensionless parameters are $b_0 = 0.003$, $a = 0.02$ and $\gamma = 0.01$. Following an electron run over several ion gyroperiods is expensive, so we use the fact that time and ψ_0 are equivalent to 'take snapshots' of the system at different times.

This particular run was divided into two parts. In the first we use $\psi_0 = 4.0 \times 10^{-4}$, which places the system $17.7\,T_{0i}$ before the appearance of the neutral line and in the second we use $\psi_0 = 6.0 \times 10^{-4}$, which places the system $22.8\,T_{0i}$ after the appearance of the neutral line. We will henceforth disregard the value of ψ_0, and refer to the two parts of the run by the equivalent time label. The run at $t = -17.7$ for instance, or the early run, is the part with $\psi_0 = 4.0 \times 10^{-4}$. Similarly the late run is the part with $\psi_0 = 6.0 \times 10^{-4}$. In both cases the initial distribution was flat in both configuration and velocity space, with $v'_j = 1.4 \times 10^{-4}$, which is equivalent to an initial temperature of $5 \times 10^{-5}\,keV$.

Both parts of the electron run are similar with the late (post neutral line) run developing quicker, and having consistently a much higher current and temperature, as expected. The main difference in the two runs, which shows most dramatically the effect of the neutral line, is the time history of the in-phase current $\langle \hat{j} \cdot \hat{E} \rangle$. For the early electron run, the value of $\langle \hat{j} \cdot \hat{E} \rangle$ is plotted against time in Fig. (5)-a, and for the late run in Fig. (5)-b. Because of the similarity of the plots in the beginning, it it fair to assume that during that time the system is reaching its 'preferred state', while after the initial 'equilibration' we can see the real response of the system. In the early run $\langle \hat{j} \cdot \hat{E} \rangle$ reaches a constant value (except for small oscillations), while in the late run it increases almost linearly in time. Since the only difference in the two runs is the existence of the neutral line in the late run, we see that the appearance of the neutral line causes the value of the height-integrated $\langle \hat{j} \cdot \hat{E} \rangle$ to increase rapidly with time. Again the picture is insensitive to initial conditions. In addition, an otherwise identical pair of runs with a modest amount of velocity-space diffusion ($D_v = 0.6\ km^2/s^3$) added in the form of random 'kicks' in the particle velocity, exhibited virtually identical behavior, as can be seen in Figs. (5)-c,d. A number of runs was made with different initial conditions, both flat and gaussian, and velocity-space diffusion coefficients as high as $1.6\ km^2/s^3$, and they all showed the same basic qualitative features with the corresponding run that had no velocity space diffusion.

We therefore see that single particle dynamics can give realystic results for the magnetotail evolution, and that the neutral line plays an important role in this evolution. Two important questions remain however.

1) Is the particle energization truly irreversible, or are we observing some 'sloshing' mode, and the particles will give up their energy back to the fields once the direction of the electric field is reversed, and

2) How will collective effects change our results? In particular, will the waves become depleted as their energy is imparted to the particles and the growth slow down, or will, conversly, the currents produced by the particles reinforce the waves? This question becomes particularly important when it is observed that the background current density is $(c/4\pi)\vec{\nabla} \times \vec{B} \approx 2.5 \times 10^{-3}\ \mu A/m^2$, much smaller that the currents produced by the ions (cf. Fig. (2), the scale current is $j_0 = 1.55\ \mu A/m^2$) although still much higher than those produced by the electrons (cf. fig. (5)). In addition, the current is now flowing over a much narrower channel in z (cf. Fig. 2). When the difference in the width of the current channels is taken into account, the total ion current is still comparable to the total MHD current, but no longer dominant.

The first question is partly addressed by the $v_\perp$–$v_\parallel$ plots in Fig. (4). The second question can of course be fully addressed only in the context of a fully self consistent simulation. However, the method we use to show the irreversibility of particle heating, can also be employed to provide some useful, albeit imperfect, insight into the question of collective effects.

In order to show that the particle heating is irreversible, we introduce an explicit time dependence in the amplitude of the tearing mode. We do this in two different ways, and the results we obtain are identical for both methods. In the first method we put

$$\psi_0 \rightarrow \psi_0 \sin(\omega t) \qquad (13a)$$

in Eq. (1), which, if we also choose $\gamma = 0$, gives

$$B_z = B_0 b_0 + B_0 \psi_0 k \sin(kx)\sin(\omega t)$$
$$E_y = B_0 \psi_0 \frac{\omega \cos(\omega t)}{c} \cos(kx) \tag{13b}$$

If we now choose ω and ψ_0 appropriately and stop our simulation at $\omega t = \pi/2$, the electric field has changed direction half way through the run (before or after the appearance of the neutral line, depending on the value of ψ_0), while the magnetic field has maintained the same direction throughout the run (the magnetic island increases at first and then decreases, but the field topology remains unchanged). In the second method, we put

$$\psi_0 \rightarrow \psi_0 e^{\alpha t^2} \tag{14a}$$

in Eq. (1), which gives

$$B_z = B_0 b_0 + B_0 \psi_0 k \sin(kx) e^{\alpha t^2 + \gamma t}$$
$$E_y = B_0 \psi_0 \frac{(2\alpha t + \gamma)}{c} \cos(kx) \tag{14b}$$

By appropriately choosing the values of α and γ, we can arange for the electric field to change direction (at $t_r = -\gamma/2\alpha$) before or after the appearance of the neutral line (at $t_c = (1/\gamma)\ln(b_0/k\psi_0)$, cf Eq. 3) without changing the topology of the magnetic field. Several runs were made with these two different methods, using different initial conditions, and the results confirm that the heating is indeed irreversible. Although the heating rate was substantially reduced, and even stopped, after the electric field changed direction, the particles retained the temperatures they had already attained, demonstrating that stochasticity can indeed lead to thermalization of the particle energy, rather than just streaming.

The question of depletion or reinforcement of the wave by the particle currents is equivalent to the question of what is the proper growth rate of the tearing mode, since

there is no fundamental difference between a time dependent amplitude, and a different mode growth rate. Any algebraic time dependence will, of cource, be quickly masked by the exponential. A simple exponential dependence is equivalent to running different values of γ, since we can put $\gamma = \gamma_1 + \gamma_2$ and adopt the view that the wave is growing as $e^{\gamma_1 t}$ while its amplitude changes as $e^{\gamma_2 t}$. We used a number of different values for γ, in the range $0.005 \leq \gamma \leq 0.05$. The heating rate was slightly lower for lower γ's, the final temperatures were also lower (eg. ~ 1 keV for $\gamma = 0.005$ and 3.8 keV for $\gamma = 0.05$ for two otherwise identical runs), and the timescales were different as expected (we had to integrate for longer times to obtain similar results), but the overall picture remained unchanged. In particular the relative importance of the neutral line remained the same for all values of γ.

An intuitively more obvious, although still rudimentary, way of addressing the question is to use the second method mentioned above for the irreversibility of heating, by viewing the $e^{\alpha t^2}$ time dependence as originating from the amplitude of the tearing mode (Eq. 14a). A negative value of α would then correspond to a wave being depleted by transfering its energy to the particles, while a positive α would correspond to the particle currents reinforcing the wave. Several values of α were used in the range $-0.001 \leq \alpha \leq 0.01$, and the results were similar to the ones obtained by running different values of γ, as expected. The only significant difference was that, for $\alpha < 0$, the electric field can change direction at $t_r = -\gamma/2\alpha$ as mentioned above. If the reversal happens before the neutral line appears ($t_r < t_c$) the final state is characterized by lower temperatures and streaming velocities than if the reversal happens after the appearance of the neutral line ($t_r > t_c$).

Conclusions

We see that the simple current sheet system we study here, which models the magnetotail fields by a Harris sheet with a small normal magnetic field component and a tearing perturbation added, and only considers the response of charged particles to these fields,

with no collective effects present other than the ones implicit in the use of the tearing mode, appears to describe correctly several features of the magnetotail plasma. Particle temperatures and bulk earthward drift velocities, both in the plasma sheet and in the PSBL, are in good agreement with the observed values, and the neutral line is seen to play an important role in the development of the tearing mode. The system also seems to always end up in the neighborhood of the same state shortly before the time the neutral line appears, and the further from that state it is when we start the simulation, the faster it will converge to it. This state appears to be characterized by $\kappa \lesssim 1$. For runs that start with $\kappa \gg 1$, the value of κ is drastically reduced in a very short time (one particular run went from $\kappa \approx 40$ to $\kappa \approx 0.6$ in less than $0.05\,T_{0i} = 0.16\,sec$) and then remains more or less unchanged, with $\kappa \lesssim 1$. Since $\kappa = b\sqrt{a/\rho_0} \sim E^{-1/4}$, this is consistent with the evolution of the temperature as was discussed in Section-III. If we start with a higher temperature, so that the initial κ is less than one, there is less heating and the final temperature is again within the observed values, with $\kappa \lesssim 1$. Finally we have shown that orbital stochasticity can lead to the broadening of the particle distribution function and hence irreversible heating, and that a time dependent tearing mode amplitude has no effect on the results, particularly on the importance of the neutral line in the evolution of the magnetotail.

The present work is confined to a zero cross-tail magnetic field component B_y. This is not always true in the magnetotail, and there are indications (Tajima, 1981) that a nonzero B_y may inhibit the tearing mode, by magnetizing the electrons. This is clearly an important point that needs to be further clarified. The present work also does not address the trigger mechanism, nor can it properly treat the effect of the generated currents back onto the fields, although it suggests that neither a partial depletion, nor a reinforcement of the mode by the particle currents will introduce a qualitative change to our results. This is still an important question however, since the observed ion current densities are of the order of several $\mu A/m^2$, much greater than the background current density, $j_b \approx 2.5 \times 10^{-3}\ \mu A/m^2$

(although confined to a much smaller current channel). The observed *electron* current densities however are much smaller, of the order of 10^{-5} $\mu A/m^2$. This suggest that the resolution of the point may be related to the work of Lembége and Pellat (1982), who showed that the adiabaticity of the electrons will also stabilize the *ion* tearing mode. If that work can be extended to show that the nonadiabaticity of the electrons can actually be viewed as a 'valve' that regulates the flow of free energy in the system, the ion current densities we observe will no longer present a problem.

The fact that a test particle code with a simple model for the electromagnetic fields of the geomagnetic tail give such realistic results, and the fact that these results are insensitive to initial conditions, or even to a small amount of velocity-space diffusion, lends support to the proposition put forth recently (Coroniti, 1985a,b; Büchner and Zelenyĭ, 1986, 1987; Martin, 1986) that stochastic particle dynamics in the magnetotail is an important ingredient of the tail behaviour. While self-consistent field effects are important in determining the global form of the electromagnetic perturbation of the geomagnetic tail as given by resistive MHD simulations, the rate of dissipation of the released magnetic energy and the rate of particle heating depend on the single particle processes discused here.

Acknowledgements

One of us (I.D.) wishes to thank T.W. Speiser and P.B. Dusenbery for many fruitfull discussions on the magnetotail observational data. This work supported by US Department of Energy grant #DE-FG05-80ET 53088, NSF grant #ATM-8703301 and NASA grant #NAGW-1176. Computer time provided by the National Magnetic Fusion Energy Computer Center and the San Diego Supercomputer Center.

REFERENCES

Anderson, R.R., Plasma waves at and near the neutral sheet, Proceedings of the conference on Achievements of the IMS, *Eur. Space Agency Spec. Publ.*, ESA SP-217, 199, 1984.

Büchner, J. and L.M. Zelenyĭ, Deterministic chaos in the dynamics of charged particles near a magnetic field reversal, *Phys. Lett. A* 118, 395, 1986.

Büchner, J. and L.M. Zelenyĭ, Chaotisation of the electron motion as the cause of an internal magnetotail instability and substorm onset, *J. Geophys. Res.* 92, 13456, 1987.

Chen, J. and P. Palmadesso, Chaos and nonlinear dynamics of single-particle orbits in a magnetotail-like magnetic field, *J. Geophys. Res.* 91, 1499, 1986.

Coppi, B., G. Laval and R. Pellat, Dynamics of the geomagnetic tail, *Phys. Rev. Lett.* 16, 1207, 1966.

Coroniti, F.V., On the tearing mode of quasineutral sheets, *J. Geophys. Res.* 85, 6719, 1980.

Coroniti, F.V., Explosive tail reconnection: the growth and expansion phases of magnetospheric substorms, *J. Geophys. Res.* 90, 7427, 1985a.

Coroniti, F.V., Space plasma turbulent dissipation: Reality or myth?, *Space Sci. Rev.* 42, 399, 1985b.

DeCoster, R.J. and L.A. Frank, Observations pertaining to the dynamics of the plasma sheet, *J. Geophys. Res.* 84, 5099, 1979.

Doxas, I., Two case studies of stochastic transport: anomalous transport in two drift waves and collisionless reconnection, Ph.D. thesis, University of Texas at Austin, 1988.

Drake, J.F, and Y.C. Lee, Kinetic theory of tearing instabilities, *Phys. Fluids* 20, 1341, 1977.

Dungey, J.W., Interplanetary magnetic field and the auroral zones, *Phys. Rev. Lett.* 6, 47, 1961.

Dusenbery, P.B., R.R. Anderson, D.G. Mitchell and T.W. Speiser, Substorm associated wave turbulence: a study of the CDAW 6 substorm, preprint, 1989.

Eastman, T.E., L.A. Frank, W.K. Peterson and W. Lennartsson, The plasma sheet boundary layer, *J. Geophys. Res.* 89 A3, 1553, 1984.

Eastwood, J.W., Consisitency of fields and particle motion in the Speiser model of the current sheet, *Planet. Space Sci.* 20, 1555, 1972.

Eastwood, J.W., The warm current sheet model and its implications on the temporal behaviour of the geomagnetic tail, *Planet. Space Sci.* **22**, 1641, 1974.

Esarey, E. and K. Molvig, A turbulent mechanism for substorm onset in the earth's magnetotail, *Geophys. Res. Lett.* **14**, 367, 1987.

Furth, H.P., J. Killeen and M.N. Rosenbluth, Finite resistivity instabilities of a sheet pinch, *Phys. Fluids* **6**, 459, 1963.

Galeev, A.A. and L.M. Zelenyĭ, Tearing instability in plasma configurations, *Sov. Phys. JETP* **43**, 1113, 1976.

Galeev, A.A., Reconnection in the magnetotail, *Space Sci. Rev.* **23**, 411, 1979.

Gear, W., Numerical initial value problems in ordinary differential equations, *Prentice Hall*, Englewood Cliffs, N.J., 1971.

Hagege, K., G. Laval and R. Pellat, Interaction between high-frequency turbulence and magnetospheric micropulsations, *J. Geophys. Res.* **78**, 3806, 1973.

Harris, E.G., On a plasma sheeth separating regions of oppositely directed magnetic field, *Nuovo Cimento* **23**, 115, 1962.

Huang, C., Private comunication, 1989.

Huba, J.D., N.T. Gladd and K. Papadopoulos, Lower hybrid drift wave turbulence in the distant magnetotail, *J. Geophys. Res.* **83**, 5217, 1978.

Kim, J.-S. and J. Cary, Charged particle motion near a linear magnetic null, *Phys. Fluids* **26**, 2167, 1983.

Laval, G., R. Pellat, and M. Vuillement, Instabilites electromagnetiques des plasmas sans collisions, IAEA, VIENNA, 1965.

Lembège, B., and Pellat, Stability of a thick two-dimentional quasineutral sheet, *Phys. Fluids* **25**, 1995, 1982.

Lyons, L.R., Electron energization in the geomagnetic tail current sheet, *J. Geophys. Res.* **89**, 5479, 1984.

Lyons, L.R. and T.W. Speiser, Ohm's law for a current sheet, *J. Geophys. Res.* **90**, 8543, 1985.

Lyons, L.R. and A. Nishida, Description of substorms in the tail incorporating boundary layer and neutral line effects, *Geophys. Res. Lett.* **15**, 1337, 1988.

Lyons, L.R. and T.W. Speiser, Evidence for current sheet acceleration in the geomagnetic tail, *J. Geophys. Res.* **87**, 2276, 1982.

Lyons, L.R. and D.W. Williams, Quantitative aspects of Magnetotail Physics, D. Reidel, 1984.

Martin, R.F.,Jr., Chaotic particle dynamics near a two-dimensional magnetic neutral point with applications to the geomagnetic tail, *J. Geophys. Res.* 91, 11985, 1986.

Parker, E.N., Newtonian development of dynamical properties of ionized gasses of low density, *Phys. Rev.* 107, 924, 1957.

Paschmann, G., N. Sckopke and E.W. Hones, Jr., Magnetotail plasma obeervations during the 1054 UT substorm on March 22, 1979 (CDAW 6), *J. Geophys. Res.* 90, A2, 1217, 1985.

Press, W.H., B.P. Flannery, S.A. Teukolsky and W.T. Vetterling, Numerical recipies, the art of scientific computing, *Cambridge University press*, Cambridge, 1986.

Shindler, K., Adiabatic orbits in discontinuous fields, *J. Math. Phys.* 6, 313, 1965.

Shindler, K., A theory of the substorm mechanism, *J. Geophys. Res.* 79, 2803, 1974.

Sonnerup, B.U.Ö., Adiabatic particle orbits in a magnetic null sheet, *J. Geophys. Res.* 76, 8211, 1971.

Speiser, T.W., Particle trajectories in model current sheets; 1. Analytical solutions, *J. Geophys. Res.* 70, 4219, 1965.

Speiser, T.W., Particle trajectories in model current sheets; 2. Applications to auroras using a geomagnetic tail model, *J. Geophys. Res.* 72, 3919 1967.

Speiser, T.W., On the uncoupling of parallel and perpendicular motion in a neutral sheet, *J. Geophys. Res.* 73, 1112, 1968.

Speiser, T.W., Conductivity without collisions or noise, *Planet. Space Sci.* 18, 613, 1970.

Speiser, T.W. and L.R. Lyons, Comparison of an analytical approximation for particle motion in a current sheet with precise numerical calculations, *J. Geophys. Res.* 89, 147, 1984.

Steinolfson, R.S. and G. Van Hoven, Nonlinear evolution of the resistive tearing mode, *Phys. Fluids* 27, 1207, 1984.

Tajima, T., Tearing and reconnection, Proceedings, Fusion Energy 1981, B. MacNamara ed., IAEA, 403, 1981.

Figure Captions

Figure-1

The magnetic field with 200 sample particles plotted for four different times for the ion run. (a) t=0 T_{0i}, (b) t=183.3 T_{0i}, (c) t=233.3T_{0i}, (d) t=280.0T_{0i}

Figure-2

$\langle j \cdot E \rangle$ and temperature plots for the ion run. (a, b) t=166.7 T_{0i}; (c, d) t=216.7 T_{0i}; (e, f) t=273.3 T_{0i}; (g, h) t=166.7 T_{0i}, $\langle j \cdot E \rangle$ and temperature plotted against x.

Figure-3

The earthward drift velocity v_x for the ion run, plotted for four different times. (a) t=33.3 T_{0i}, (b) t=166.7 T_{0i}, (c) t=246.7 T_{0i}, (d) t=280.0 T_{0i}

Figure-4

Contour plots of the particle distribution function for the five boxed areas of particle concetration in Fig. (3)-c. a)–d), correspond to the four peripheral areas of particle concetration, clockwise from the top left. e) corresponds to the central area, $-0.5 \leq x/a \leq 0.5$, $-0.2 \leq x/\lambda \leq 0.2$.

Figure-5

$\langle j \cdot E \rangle$ plotted against time for the electron run. (a) The early run, no velocity-space diffusion. (b) The late run, no velocity-space diffusion. (c) The early run, $D_v = 0.6\, km^2/s^3$. (d) The late run, $D_v = 0.6\, km^2/s^3$.

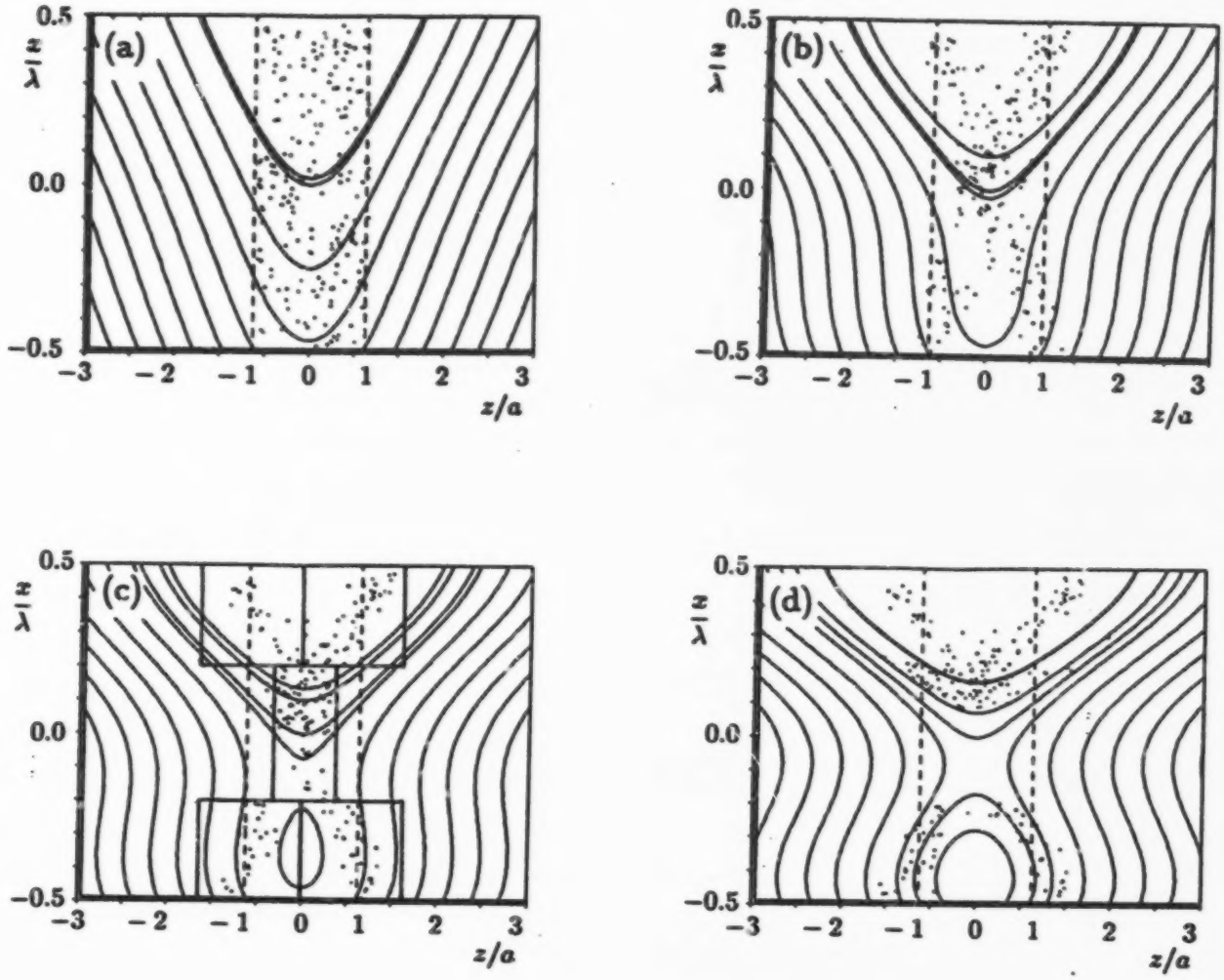

Figure-1

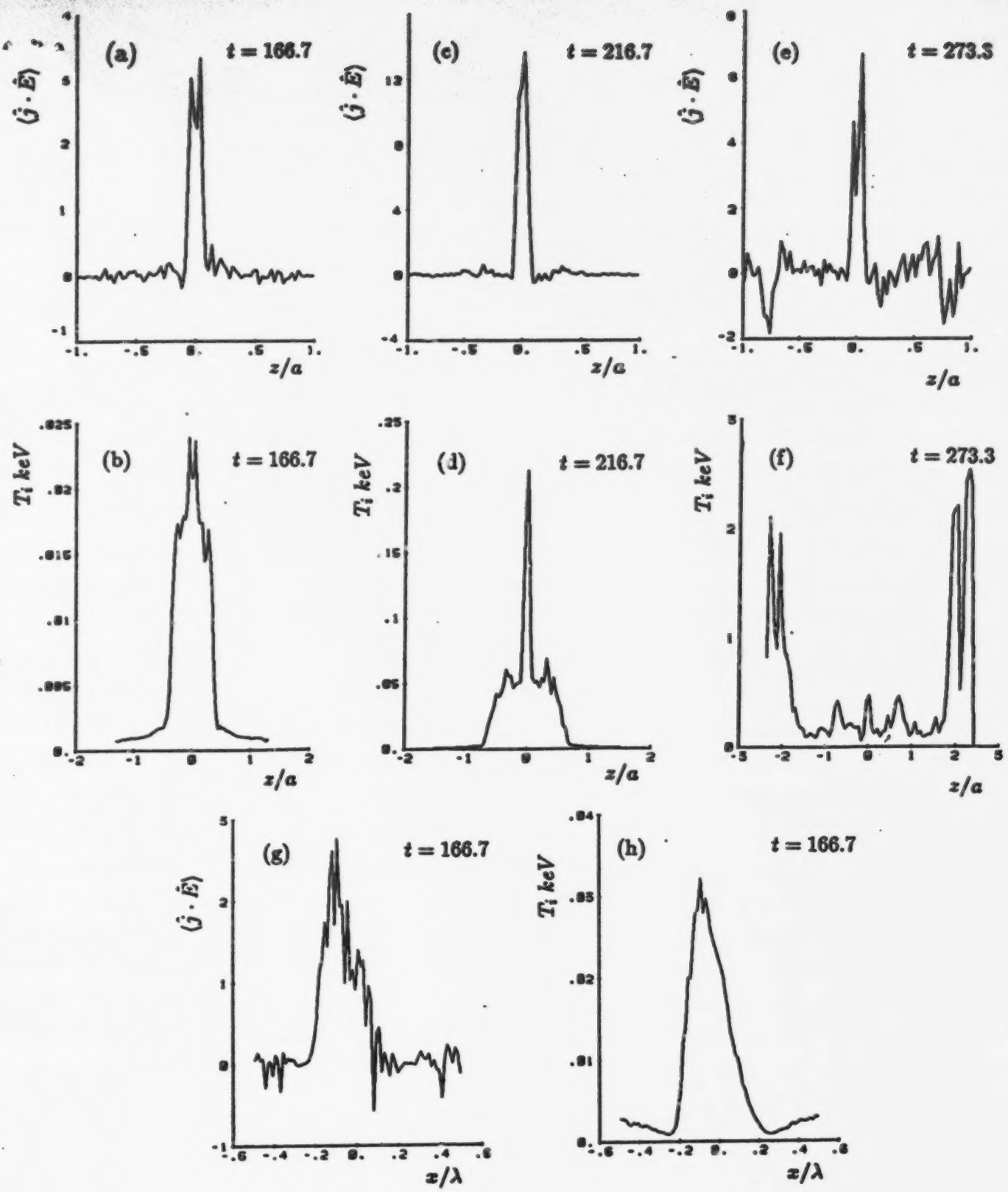
(a)
t = 166.7
$(\hat{j} \cdot \hat{E})$
z/a
(c)
t = 216.7
$(\hat{j} \cdot \hat{E})$
z/a
(e)
t = 273.3
$(\hat{j} \cdot \hat{E})$
z/a
(b)
t = 166.7
T_i keV
z/a
(d)
t = 216.7
T_i keV
z/a
(f)
t = 273.3
T_i keV
z/a
(g)
t = 166.7
$(\hat{j} \cdot \hat{E})$
x/λ
(h)
t = 166.7
T_i keV
x/λ

Figure 2

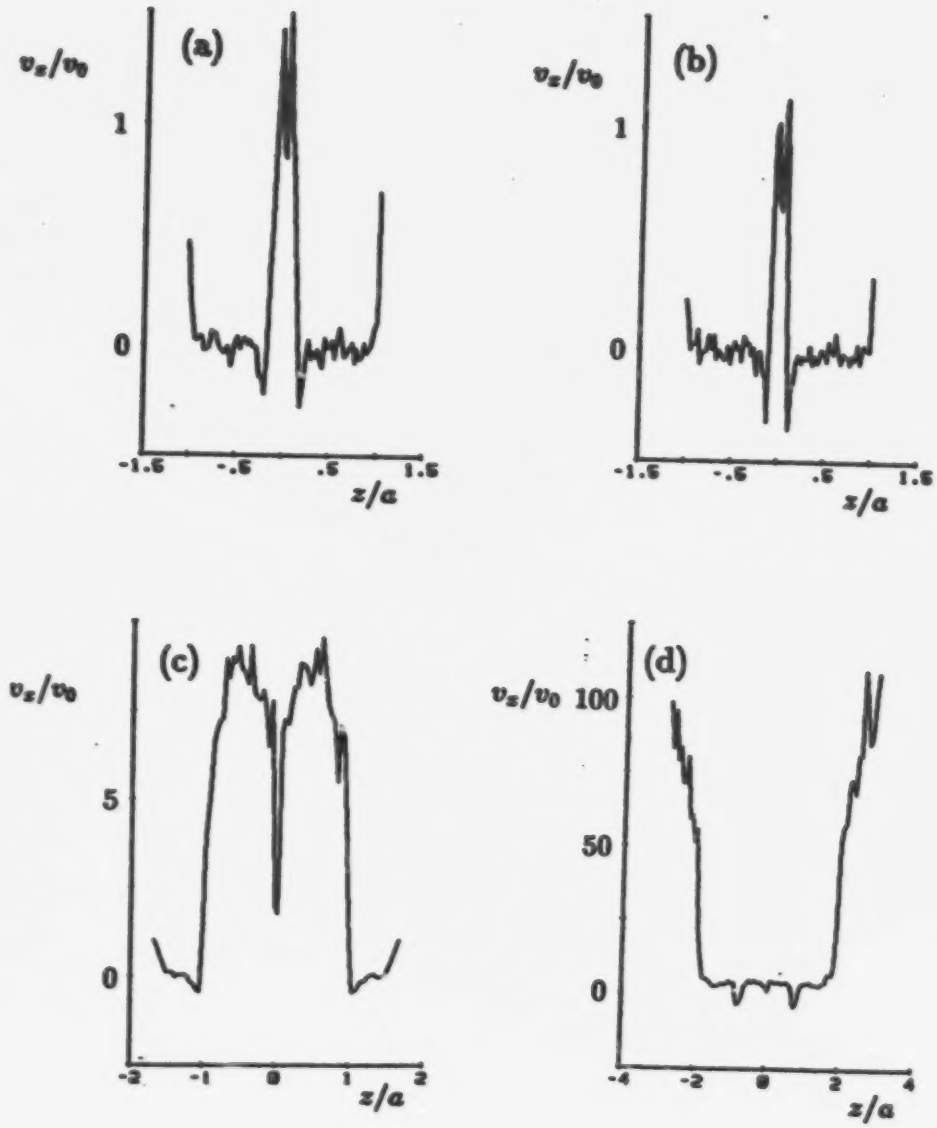
(a)
v_z/v_0
1
0
-1.5
-.5
.5
1.5
z/a
(b)
v_z/v_0
1
0
-1.5
-.5
.5
1.5
z/a
(c)
v_z/v_0
5
0
-2
-1
0
1
2
z/a
(d)
v_z/v_0
100
50
0
-4
-2
0
2
4
z/a

Figure 3

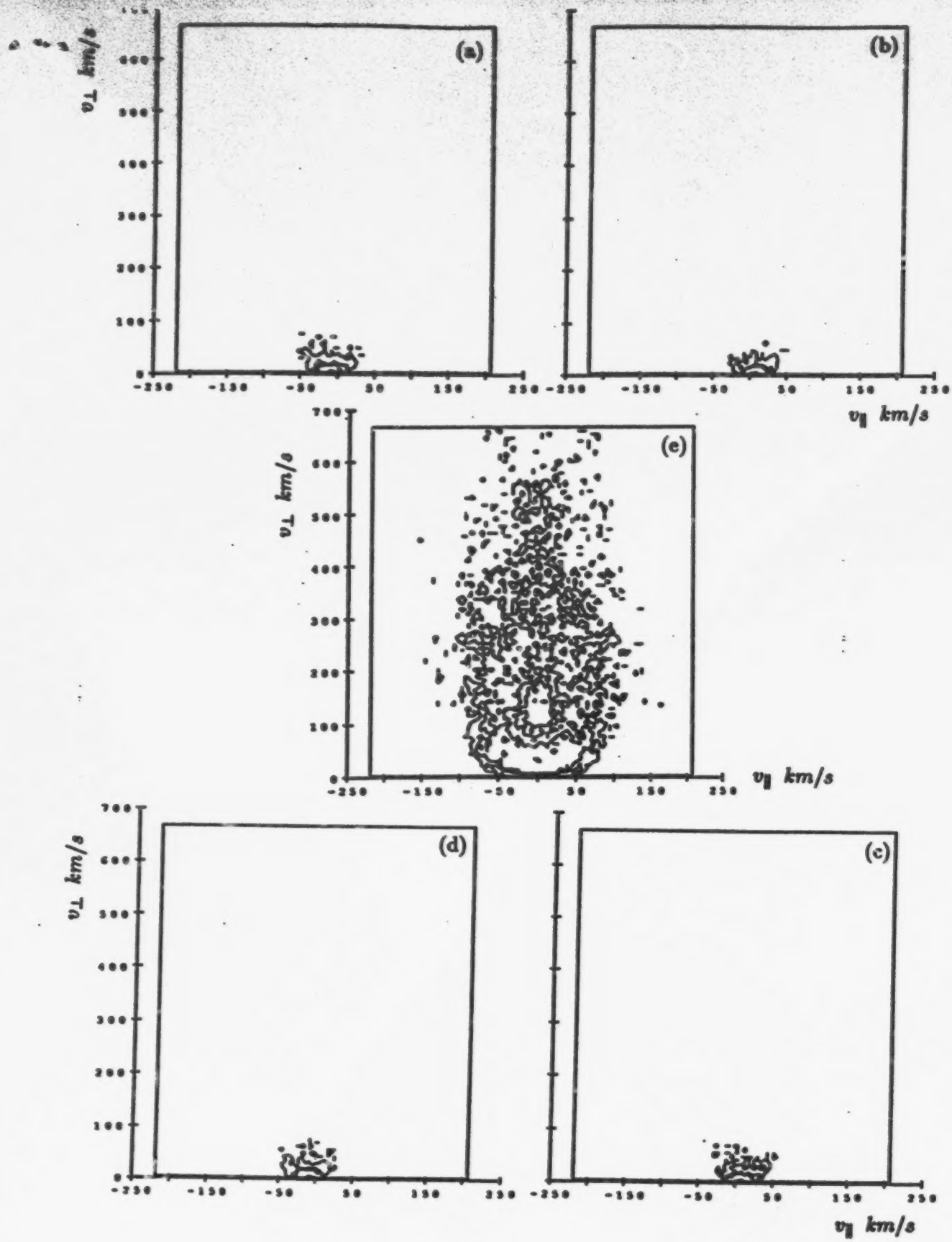
(a)
(b)
(c)
(d)
(e)
$v_\perp$ km/s
$v_\parallel$ km/s
-250
-150
-50
50
150
250
100
200
300
400
500
600
700

Figure 4

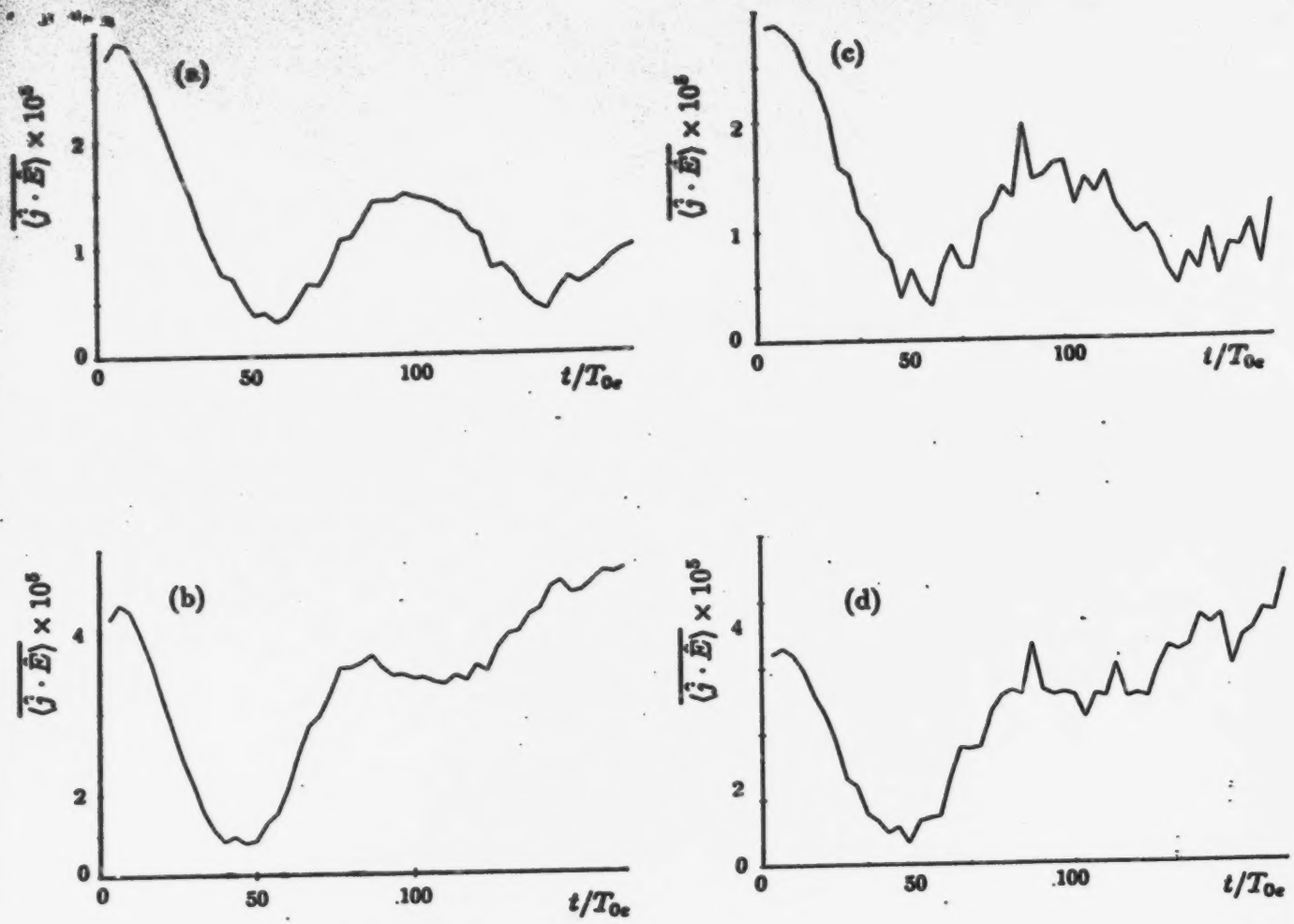
(a)
(b)
(c)
(d)
$\overline{\langle \vec{j} \cdot \vec{E} \rangle} \times 10^5$
t/T_{0e}
0
50
100

Figure 5